Failure mode of rainfall-induced landslide of granite residual soil, southeastern Guangxi province, China

Shanbai Wu[1, 2, 3, 4]**, Ruihua Zhao**[1, 2, 3]**, Liping Liao**[1, 2, 3*]**, Yunchuan Yang**[1, 2, 3*]**, Yao Wei**[1, 2, 3]**, Wenzhi Wei**[1, 2, 3]

[1]College of Civil Engineering and Architecture, Guangxi University, Nanning 530004, China;

[2]Guangxi Key Laboratory of Disaster Prevention and Engineering Safety, Guangxi University, Nanning 530004, China;

[3]Key Laboratory of Disaster Prevention and Structural Safety of Ministry of Education, Guangxi University, Nanning 530004, China;

[4]Faculty of Engineering, China University of Geosciences, Wuhan 430074, China

Correspondence: Liping Liao (01llp@163.com), Yunchuan Yang (yyunchuan@163.com)

Abstract. Granite residual soil landslides are widely distributed in the southeast of Guangxi, China. They are posing threats to local communities, economic development, and ecological restoration. To understand the failure mode of the landslide can provide a scientific basis for early warning and prevention. In this study, it conducted artificial flume model tests to investigate the failure mode of granite residual soil landslide. The macroscopic phenomena of landslides were observed and summarized. The response and variations of soil moisture content and pore water pressure were analyzed. And the discrepancies in landslide initiation were explored. The results had three aspects. (1) The response of volume moisture content was not synchronized with that of pore water pressure. Their variations were influenced by initial dry density, slope angle, and rainfall intensity. The fluctuation of pore water pressure depended on soil mechanical behavior and its diffusion. (2) The differences in the formation process of granite residual soil landslides included the initiation time and mode. The starting time of landslide was delayed with increasing initial dry density and slope angle, but shortened with increasing rainfall intensity. The failure mode could be changed from a sudden type to a progressive type due to the increase of initial dry density. (3) There are five stages in the landslide mobilization as follows: rain infiltration and crack generation, soil slide at the slope toe, occurrence of surface runoff and soil erosion, formation of steep-free surface, and soil slide at the upper slope. Above research provides valuable reference for the prevention and early warning of granite residual soil landslide in the southeast of Guangxi.

Keywords: Granite residual soil; Rainfall-induced landslide; Failure mode; Flume model test; Southeastern Guangxi

32

1   Introduction

Rainfall-induced landslides are the most common geohazards in the tropical and subtropical areas covered by granite residual soil, such as Brazil (Lacerda, 2007; Coutinho et al., 2019), Singapore (Rezaur et al., 2003; Rahardjo et al., 2008; Rahardjo et al., 2012; Zhai et al., 2016; Zhang et al., 2019), Malaysia (Rahman et al., 2018), Korea (Kim et al., 2004; Pham et al., 2019), the southern (Jiao et al., 2005; Luo et al., 2021; Liu et al., 2021; Liu et al., 2020a; Liu et al., 2020b) and southeastern China (Xia et al., 2019; Yao et al., 2021; Shu et al., 2021; Zhao et al., 2021). Guangxi is located in southeastern China, where granite is concentrated in the southeast, and landslides occur frequently (Liao et al., 2019). Hot and rainy climatic conditions have caused strong weathering of the surface granite, giving birth to tens of thousands of residual soil. This provides a superior environment for the formation of landslides. Therefore, the southeastern Guangxi has been threatened by granite residual soil landslides for a long time. Granite residual soil is a regional special soil (Ministry of Construction of the People's Republic of China, 2002). One reason is that it has the dual mechanical properties of cohesive soil and sandy soil. The other is that it exhibits an abnormal combination of poor physical properties (such as high liquid limit and large void ratio) and high-strength properties in a natural state (Chen et al., 2011). However, granite residual soil is extremely sensitive to rainfall, and is easy to disintegrate and soften, which will induce large-scale landslides (Dahal et al., 2008; Liu et al., 2020a; Zhang and Tang, 2013). Although shallow landslides are the main type (Rahardjo et al., 2008; Kim et al., 2004), they still have the characteristics of high frequency (Kim et al., 2015), suddenness and mass occurrence.

The failure mode of residual soil landslide is an important basis for disaster prevention and mitigation and early warning and prediction of landslide (Rezaur et al., 2003). In this regard, many scholars have conducted in-depth studies on granite residual soil landslide and other residual soil landslide through statistical analysis, model tests and numerical simulations. They classified the type of granite residual soil (Wu, 2006b) and studied on the physical mechanical properties (Zhu and Anderson, 1998; Chen et al., 2011; Zhang and Tang, 2013; Chen and Gong, 2014; Xia et al., 2019), engineering characteristic (Wu, 2006a; Xu et al., 2017) and microstructure (Li et al., 2017; Wang et al., 2018). The formation condition (Zhan et al., 2012; Zuo et al., 2015) and instability mode (Zhao and Hu, 2005; Dahal et al., 2008; Hu et al., 2009; Xu and Jian, 2017) of granite residual soil landslides were revealed. They found and confirmed that the failure mode of residual soil slope is different from that of homogeneous soil and rock slope, it includes arc slip, plane slip and front shear slip, but plane slip is dominant (Zhan et al., 2010; Fu et al., 2018). Its failure surface is parallel to the original slope (Kim et al., 2004). They also pointed out rainfall is the most important external triggering factor due to two aspects (Coutinho et al., 2019). One is the deepening of the wetting peak induced by rainfall infiltration (Kim et al., 2004). Second, the increase in soil water content and pore water pressure can lead to a decrease in slope stability (Gasmo et al., 2000; Rezaur et al., 2003; Rahardjo et al., 2005; Lacerda, 2007; Rahardjo et al., 2008). Thus, in the process of landslide formation, the variation of physical property parameters such as moisture, matric suction or pore pressure play an important role in the residual soil landslide (Kassim et al., 2012; Igwe and Fukuoka, 2014; Pham et al., 2019; Zhai et al., 2016). Rainfall triggered mechanisms focus on completely weathered granite fill slope in Hong Kong, China. They are static liquefaction (Chen et al., 2004) and

the transition from slide to flow due to localized transient pore water pressure (Take et al., 2004). However, static liquefaction is impossible due to unsaturated condition. Instead, local transient pore water pressure can induce the initially slip, which further triggers the high-speed slide (Take et al., 2004). Another finding is that the initial dry density (Mukhlisin et al., 2008) and slope angle (Liu et al., 2020a; Liu et al., 2020b) can affect the water permeability and control the formation of landslides (Xu et al., 2018). Many scholars have carried out related studies on the relationship between dry density of other types of soil (such as sandy soil, volcanic residual soil, and gravel soil) and the initiation of landslides. They found through model tests that the initial density can determine the stress-strain characteristics of the soil, and it corresponds to the initiation mechanism of dilation and contraction (Dai et al., 1999a; Dai et al., 1999b; Mckenna et al., 2011). The macroscopic phenomena corresponding to these two mechanisms are: saturated loose slopes will suddenly liquefy and flow quickly, while saturated dense slopes will creep slowly (Iverson et al., 2000). It can be seen that there is a significant difference in the sliding motion rate of sand landslides (Iverson, 2005). Especially when the dry density is optimal, the moving speed and sliding distance of the landslide are both maximums (Wang and Sassa, 2001). This is mainly because the initial dry density affects the soil-water interaction and soil permeability (Ng and Pang, 2000; Lin et al., 2009; Jiang et al., 2017). For example, high-density steep slopes are much more resistant to rainwater penetration than low-density gentle slopes (Xu et al., 2018). A gentle slope can lead to better accumulation of rainwater, a faster increase in water content, but a slower rate of soil collapse (Liu et al., 2020a; Liu et al., 2020b). Other scholars have further confirmed the above results through numerical simulations. That is, the initial dry density has a decisive influence on the movement accumulation and evolution process of the landslide, and there are also significant differences in the slip rate (Liang et al., 2017).

The above researches have pointed out the direction for the follow-up work. However, most of the conclusions related to failure process focus on gravel soil (Chen et al., 2017; Liao et al., 2018), sandy soil (Moriwaki et al., 2004; Huang et al., 2008; Huang and Yuin, 2010), fill slope (Chen et al., 2004; Take et al., 2004), clay soil (Elkamhawy et al., 2018) and loess slope (Tu et al., 2009). Moreover, the degree of development of granite weathering crust is closely related to the climate, topography and environment (Qu et al., 2000), its residual soil has significant heterogeneity characteristics in terms of thickness, physical and mechanical property (Rahardjo et al., 2002; Rahardjo et al., 2012). These special characteristics lead to the complex initiation modes of landslides (Calcaterra and Parise, 2005; Mukhlisin and Taha, 2012; Liu et al., 2020a; Xia et al., 2019). At present, the failure mode of granite residual soil slope in the southeast of Guangxi has not been studied, which has brought challenges to the prevention and early warning of landslides. Therefore, some scientific issues need to be solved. For example, what are the similarities and differences of the failure process of granite residual soil slope? How do the physical parameters of residual soil change? In this paper, it conducted artificial flume model tests to resolve the above issues. Firstly, the macroscopic phenomena of landslide is observed and summarized. Subsequently, the variation characteristics of soil moisture content and pore water pressure are analyzed. Finally, the differences in the initiation of rainfall-induced landslide are discussed.

2   Field site and method

2.1 Field site

Rong County is a typical high-prone area of rainfall-induced landslide of granite residual soil in southeast Guangxi (Liao et al., 2019). It is located between longitude 110°15′00″-110°53′00″ E and latitude 22°27′00″-23°07′00″ N (Fig. 1). The county covers an area of 2257 km², with an average annual rainfall 1737.4 mm a⁻¹. The rainy period is from April to September, and the rainfall in this period accounts for 78.6 % of the average annual rainfall. The area of magmatic rocks is 1260.09 km², accounting for 55.83 % of the total area of the county. The lithology is mainly granite with an area 1219.06 km².
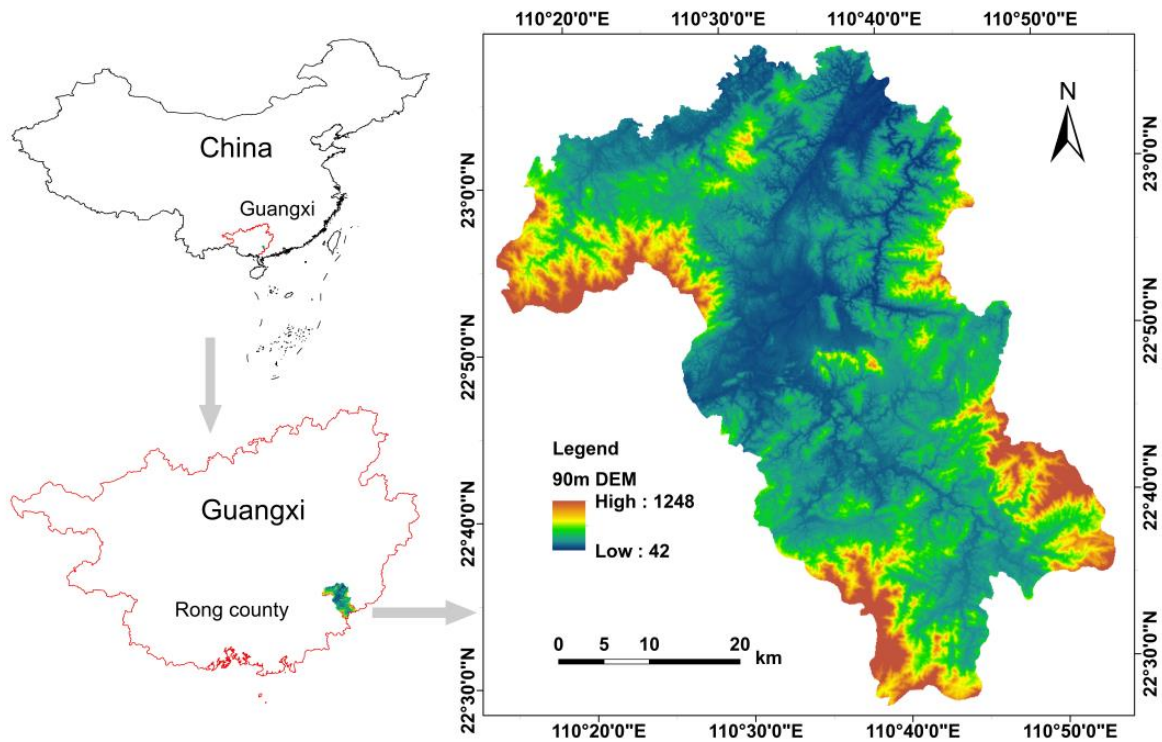
Figure 1. Study area.

2.2 Method

Longtou Village in Liuwang Town is a landslide high-prone area in Rong County. Therefore, test soil comes from Longtou village. Specific gravity of the soil is 2.71, and the minimum and maximum of dry density are 1.18 g cm⁻³ and 1.72 g cm⁻³. Particle data is the average of three sets of screen tests on granite residual soil (Fig. 2). The red grid points in Figure 2 represent the cumulative content of gravel (diameter < 2 mm) and silt and clay (diameter ≤ 0.075 mm). They are 87.52 % and 25.62 %. The angles of natural slope in the study area are 30 ° - 45 ° and mainly 40 ° - 45 °. The dry density of superficial soil is 1.20 - 1.40 g cm⁻³; and the average mass moisture content is 6 %-10 % (Wen, 2015). Only two initial dry densities of 1.20 g cm⁻³ and 1.40 g cm⁻³ are set to highlight the discrepancies between tests (Table 1). Two slope angles of 40 ° and 45 ° are established, and initial mass moisture content is controlled in the range of 6 % to 10 %. Heavy rainfall is the main factor in the formation of landslides (Wei et al., 2017). Hence, rainfall intensity and duration are set based on rainfall data

from multiple landslide events in the study area in 2010 (Wen, 2015). There are 1-3 periods of rainfall, and each period lasts for 8 hours with an interval of 15 hours. Rainfall intensities are 60 mm h^{-1} and 90 mm h^{-1} respectively. Furthermore, the groundwater level in the study area is relatively deep, the landslide initiation of granite residual soil does not depend on the fluctuation of groundwater level. Therefore, the factor of groundwater level is not considered in the tests.
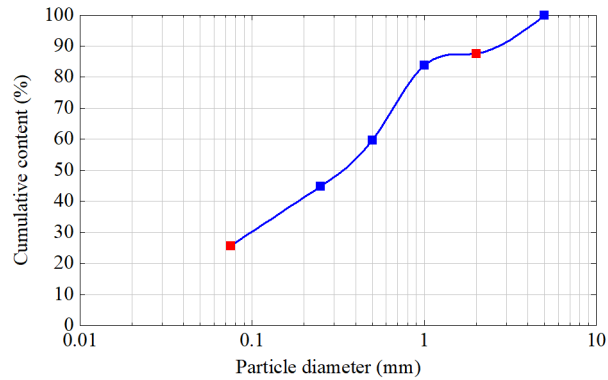
Figure 2. Particle gradation of granite residual soil.

Table 1. Scheme of artificial flume model tests.

Test number	Slope angle (°)	Initial dry density (g cm^{-3})	Rainfall intensity (mm h^{-1})	Rainfall duration (h)
1		1.20	60	8, 8, 8
2	45	1.40	60	8, 8, 8
3		1.20	90	8, 8
4		1.40	90	8, 8
5	40	1.20	60	8, 8, 8
6		1.20	90	8

Test equipments are composed of rainfall control system, data testing system, and flume model. Rainfall control system contains central control system, suction pump, water tank, hose, brace, and nozzle. The size of water output can be set in the rainfall control system. The distance from the nozzle to slope crest is 2.3 m. The effective rainfall area of the tests is 6 m^2, and the rainfall is calibrated before the formal test. Data testing system consists of sensors and data collectors (Fig. 3). The minimum unit of time for data collection is 1 min, and storage space of data collector is limited. Hence, the frequency of data collection for volume moisture content and pore water pressure is set to 1 min and 3 min respectively.
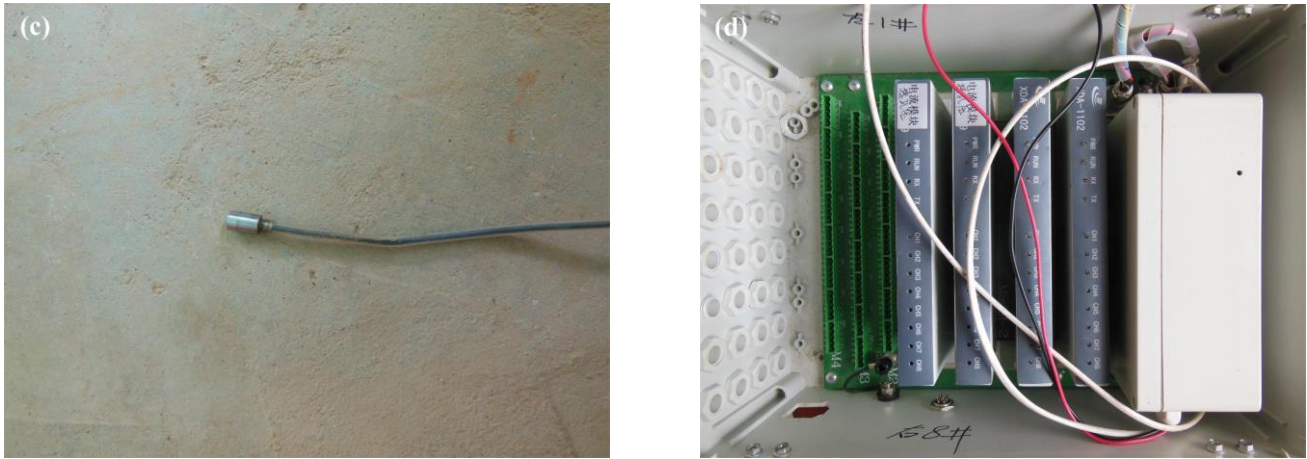
Figure 3. Testing instrument. (a) MP-406B sensor of soil moisture. (b) M-16 collector of soil moisture. (c) HC-25 micro gauge of pore water pressure. (d) MCU collector of pore water pressure.

The length, width and height of test slope are 1.5 m, 0.8 m, and 0.6 m respectively. The slope is divided into six layers, and the thickness of each layer is 0.1 m (Fig. 4). Firstly, a sufficient amount of air-dried soils are screened. Secondly, the required water is calculated based on the current and designed moisture content. Subsequently, this water is sprayed evenly into the soil. When the water and soil are fully mixed, they are placed in a container and kept for 24 hours. Finally, when moisture content of the mixture meets the requirement of designed moisture content, the slope model begins to be made. The accuracy of initial dry density must be guaranteed, so the soil of each layer is compacted with the wooden hammer. In addition, twelve monitoring points are set up inside the model. They belong to five positions. Each monitoring point consists of a soil moisture sensor and a micro gauge of pore water pressure (Fig. 4b).
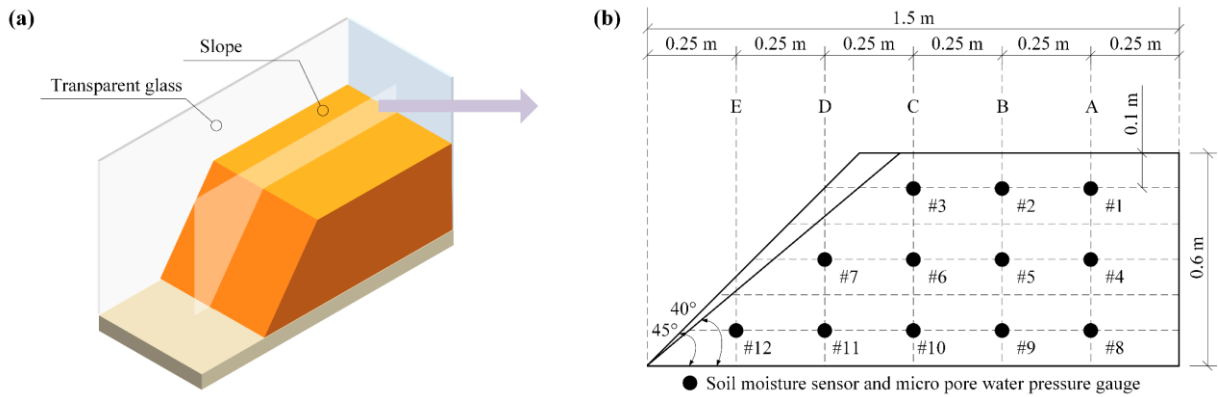
Figure 4. Flume model. (a) Three-dimensional schematic of the model. (b) Section of the slope and location of sensors.

3 Results

3.1 Macroscopic phenomena of tests

(1) Test 1

During the first rainfall, when the rainfall lasts for 50 min, two small ditches are found on the slope surface. At this time, the soil at the slope toe slips, and triggers the soil on the trailing edge to slide. The instability area is fan-shaped and located at the left side of the slope toe. Its length is three-

179 quarters of the total length of the slope. When the rainfall lasts 421 minutes, a new ditch developing
180 on the slope shoulder is connected with the original instability area. In the second rainfall, the ditches
181 are continuously eroded. At the same time, many fine particles are moved to the slope toe by rain.
182 When the rainfall lasts for 559 min, the soil of the left slope shoulder begins to slide, causing the
183 formation of tensile crack at the slope crest. Then the soil around the crack slips and accumulates to
184 the slope toe. During the third rainfall, the continuous soil slide leads to the occurrence of a steep
185 free surface. When the rainfall lasts for 1324 min, the soil of the steep surface starts to slide. The soil
186 sliding does not stop until the slope gradient becomes gentle.

187 (2) Test 2

188 When the first rainfall lasts for 67 min, the soil on the left side of the slope toe begins to slip. The
189 area of sliding range gradually extends. When the rainfall lasts 431 minutes, the instability range has
190 been extended to the slope shoulder, and the seventh sensor is exposed. Subsequently, the soil on the
191 right side of the slope toe slips, causing the soil slide in the middle of slope. During the second
192 rainfall, tiny cracks are found on the right side of slope. When the rainfall lasts for 524 minutes, the
193 soil around the crack slips, and the sliding surface is arc-shaped. Owing to continuous rainfall, the
194 process of soil slide occurs repeatedly, and the gullies forms. The slope surface is eroded by third
195 rainfall. The ditch on the right side of slope extends and the slope eventually stabilizes.

196 (3) Test 3

197 In the first rainfall process, when the rainfall lasts for 32 minutes, tensile cracks appear
198 successively on the slope toe, and the soil around the cracks slips (Fig. 5a). Subsequently, a steep free
199 surface is formed. When the rainfall lasts for 39 minutes, the soil in the middle slope begins to slide
200 (Fig. 5b). When the rainfall lasts for 215 minutes, the soil on the slope shoulder starts to slip due to
201 unbalance internal forces (Fig. 5c). It causes the sensor #3 to deviate from the embedded position.
202 When the second rainfall lasts for 811 min, blocky soil slides suddenly on the right slope toe (Fig.
203 5d). When the rainfall lasts for 923 min, massive soil on the right slope shoulder begins to slides
204 owing to the unloading effect of the slope toe (Fig. 5e). Subsequently, the slope is stable (Fig. 5f).
205 This sliding process is accompanied by the sinking of the slope.

206 (4) Test 4

207 When the first rainfall lasts for 45 min, the soil on the left slope toe starts to slip. Muddy water
208 flows from the area of sliding soil. When the rainfall lasts for 78 min, the area of instability soil
209 extends to the slope shoulder. However, only a small amount of soil on the right slope toe slips.
210 During the second rainfall, the right slope is scoured away by rain, which results in a deep gully.
211 When the rainfall lasts for 496 min, the soil on the right side of slope slips, but the slide scale is small.
212 The slope is not completely destroyed.

213 (5) Test 5

214 When the first rain lasts for 26 minutes, the soil on the right foot begins to slide. The failure range
215 extends to the middle of slope as the rainfall continues. At the same time, rainfall gravity leads to the
216 formation of low-lying areas. When the rainfall duration is 208 min, the sunken area becomes larger,
217 and the soil at the slope toe has basically slipped. When the second rainfall lasts for 766 minutes, the
218 low-lying areas are connected, and a steep free surface is formed. Subsequently, the soil at the slope
219 toe continues to slide. In the third rainfall, a small amount of soil slips. However, there is no
220 significant change in the slope eventually.

(6) Test 6

When the rainfall lasts for 5 min, tensile cracks occur at the slope toe, resulting in the soil failure. When the rainfall lasts for 27 min, the failure range extends to the shoulder of slope. Subsequently, massive soil on the free surface slides from time to time. When the rainfall lasts for 96 min, the soil in the middle of slope begins to slip, causing the exposure of sensor #7. When the rainfall lasts for 133 min, the soil on the left slope shoulder begins to slide. The slope begins to be sinking. When the rainfall lasts for 220 min, the soil on the right slope toe continues to slide. The failure area extends to the middle of slope as the rainfall continues. At the end of the rainfall, the soil on the right slope shoulder remains stable.
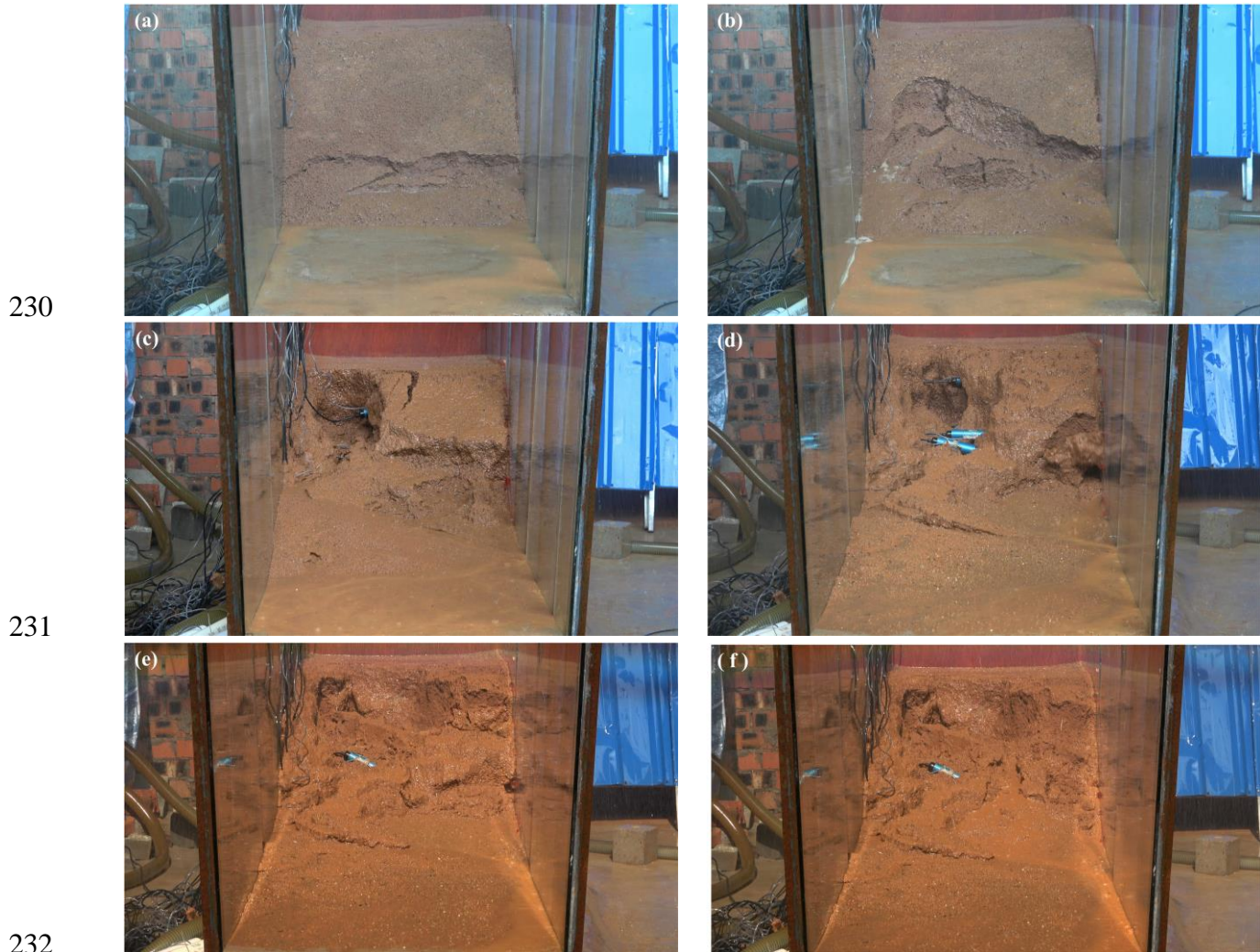
Figure 5. Typical phenomena of test 3. (a) The soil at the slope toe begins to slip after tensile cracks appear. (b) The soil in the middle slope slides. (c) The soil on the slope shoulder slips owing to unbalance internal forces. (d) Blocky soil slides suddenly on the right slope toe. (e) Massive soil on the right slope shoulder slides due to the unloading effect of the slope toe. (f) The slope is stable at the end of the rainfall.

3.2 Volume moisture content

A-E inside the flume model represents the crest, shoulder, middle, and foot of the slope respectively. The variation characteristics of the volume moisture content (VMC) at A, B, and C are relatively similar. Therefore, the VMC of C is selected in the paper to indicate a general trend. In addition, the three positions (C, D, and E) are close to the sliding surface. Thus, the data of these three positions

242   are analyzed in this section and shown in Figure 6-Figure 11. The general variation of VMC mainly
243   consists of three stages: initial constant, significant increase, and stability. When the monitoring
244   depth of the same position increases from 0.1 m to 0.5 m, the response time of VMC is delayed, but
245   the stable value of VMC increases. It is attributed to the rainwater infiltration process and its
246   accumulation. In addition, VMC is reduced due to water evaporation during the interval between two
247   rainfall periods. This phenomenon is particularly obvious for soils with a depth of 0.1-0.3 m. VMC
248   can be restored to the previous level or even higher value in subsequent rain.

249   Figure 6 and Figure 7 shows the differences of VMC between test 1 and test 2 as follows. (1)
250   When the monitoring depth of the position C is 0.1 m and 0.3 m, the stable value of VMC of test 1 is
251   smaller than that of test 2. The main reason is that the capacity of soil to store water can be enhanced
252   as initial dry density (IDD) increases (Lu et al., 2018). (2) VMC of three depths in the position C of
253   test 2 is similar. However, the VMC between three depths of test 1 has great difference. It is
254   especially noticeable in the first rain. (3) When the depth is 0.5 m, the VMC of the slope foot in test 1
255   is significantly smaller than that of the slope middle, but the VMC at these two locations is similar in
256   test 2.
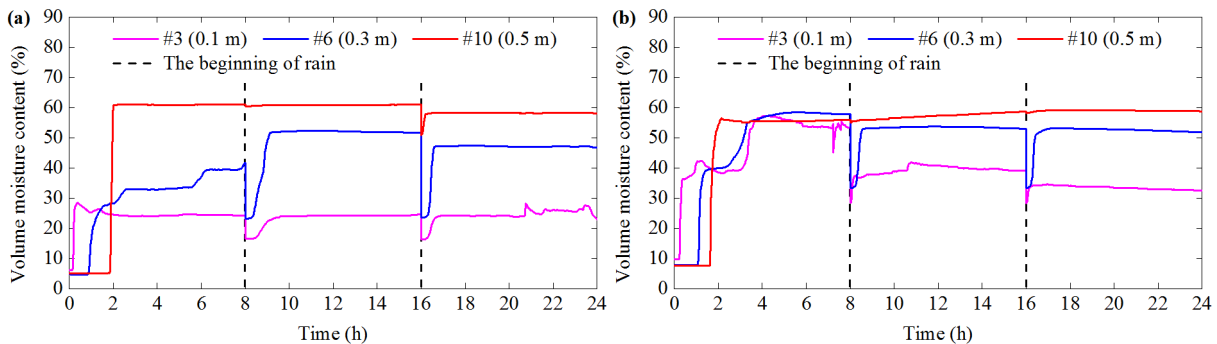
257
258 Figure 6. Volume moisture content in position C of (a) test 1 and (b) test 2.
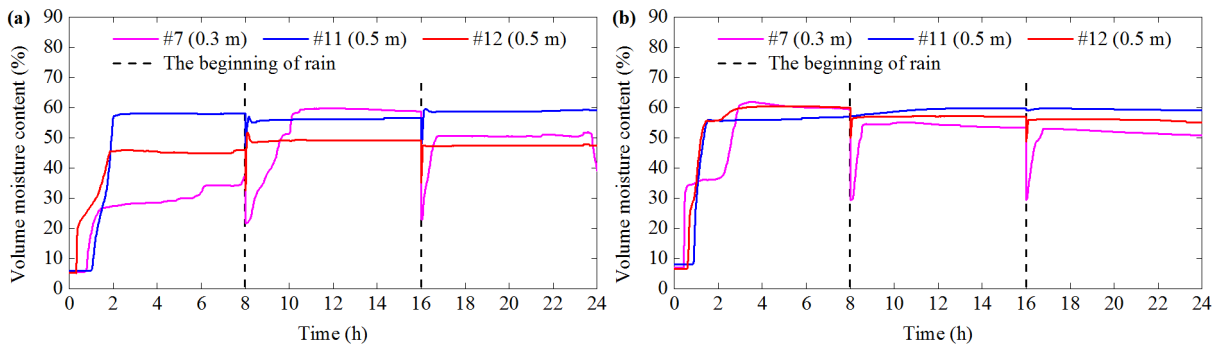
259
260 Figure 7. Volume moisture content in positions D and E of (a) test 1 and (b) test 2.

261

262   The VMC of test 3 and test 4 is shown in Figure 8 and Figure 9. The response time of VMC of test
263   3 is shorter than that of test 4 at the same location. The reason is that the increase of IDD of the soil
264   results in the weakening of rain infiltration (Lee et al., 2005). The VMC at a depth of 10 cm in test 3
265   decreases sharply and eventually becomes zero in the first rain (Fig. 8a). This is due to the soil
266   sliding causing the third sensor to deviate from its original position. In addition, the VMC at the
267   depth of 0.3 m in positions C and D of test 3 fluctuates significantly (Figs. 8a and 9a). The
268   macroscopic phenomena in section 3.1 indicate the time of the soil failure is basically corresponding
269   to the fluctuation time. Thus, the fluctuation is attributed to the soil failure. The maintenance of water

270 pipe causes a short water stop. Hence, VMC fluctuates at the beginning of the second rainfall in test
271 4 (Figs. 8b and 9b).
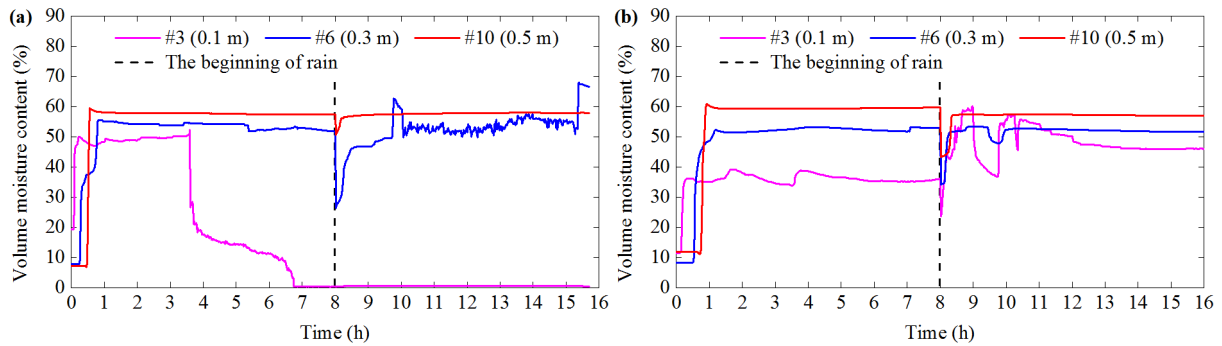
272
273 Figure 8. Volume moisture content in position C of (a) test 3 and (b) test 4.
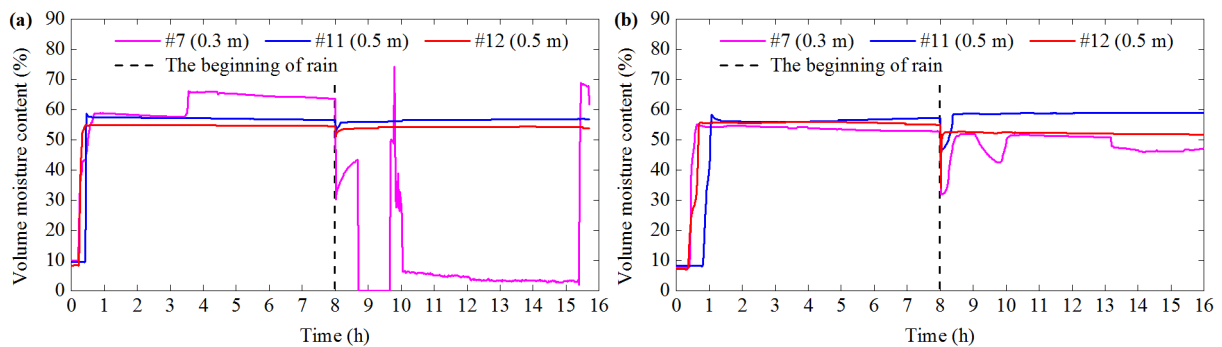
274
275 Figure 9. Volume moisture content in positions D and E of (a) test 3 and (b) test 4.
276

277 The VMC of test 5 and test 6 is shown in Figure 10-Figure 11. When the rainfall intensity
278 increases from 60 mm h^{-1} to 90 mm h^{-1}, the stable value of VMC of test 5 is less than that of test 6.
279 However, the VMC in test 6 has a longer response time than that in test 5. It is obvious in the slope
280 crest, such as the position C. The worth noting in section 3.1 is that the sliding time of test 6 is earlier
281 than that in test 5. The main reasons of the above abnormal phenomena are including three aspects.
282 One is that when the rainfall intensity is relative larger, more rainwater can penetrate the soil quickly.
283 Shallow layer can be saturated. This process can cause silt and clay to migrate vertically and
284 accumulate at a certain depth (Fang et al., 2012). Subsequently, the microstructure of soil is changed
285 (Chen et al., 2018), and the infiltration path is blocked by the fine particles. Furthermore, rainwater
286 cannot infiltrate the soil smoothly, and causes the long response time of VMC at the slope crest. The
287 other is that rainfall infiltration can cause a difference in water pressure between the slope crest and
288 the slope foot; this effect of seepage force will cause the slope foot to slide first (Zhou et al., 2014).
289 In test 5 and test 6, the soil failures are both found in the slope foot at the beginning of rainfall. It is
290 consistent with the research made by Zhou et al. (2014). This local deformation of the slope can
291 cause internal force unbalance and soil microstructure change. The rainfall infiltration will be
292 affected later (Chang et al., 2021). On the other hand, the tensile crack of the slope toe can provide a
293 preferential path of rainwater. It is the main reason for the relative early sliding time in test 6.
294 However, the sensor #12 cannot observe this data because it is not located under the crack.
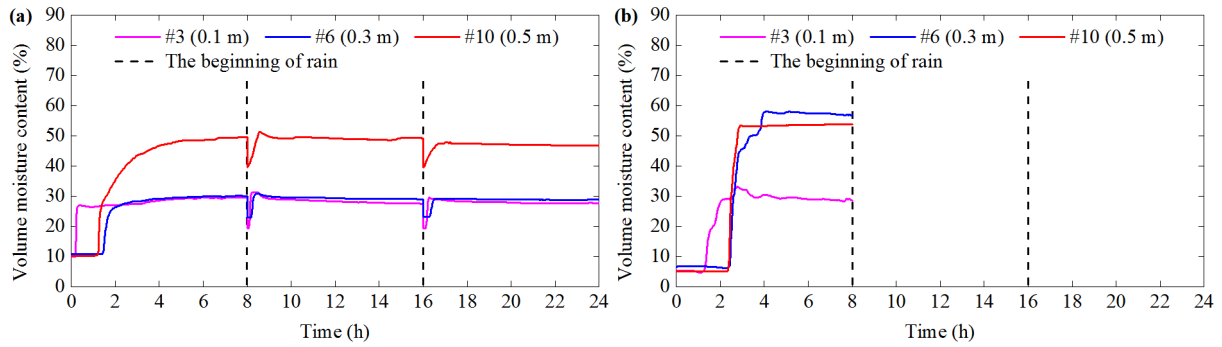
Figure 10. Volume moisture content in position C of (a) test 5 and (b) test 6.
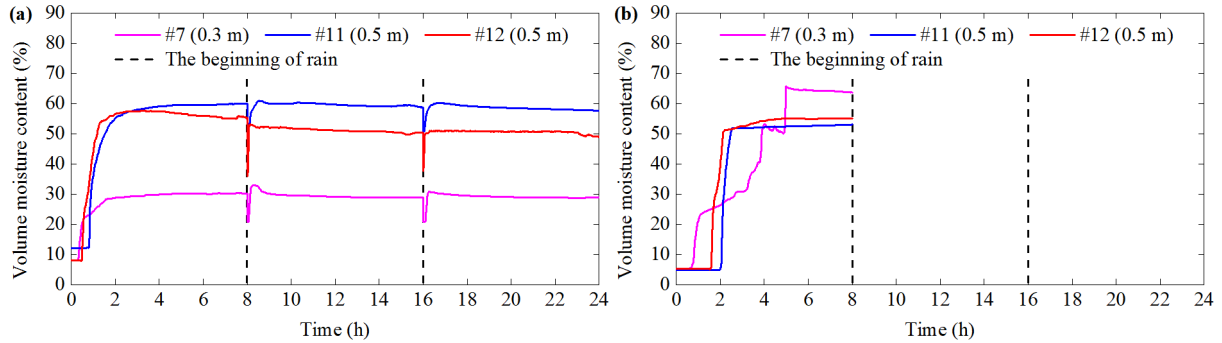
Figure 11. Volume moisture content in positions D and E of (a) test 5 and (b) test 6.

Figure 12 shows the response time and stable value of VMC at five positions during the first rainfall. Test 1and Test 2, Test 3 and Test 4 in Figure 12 are respectively compared. The similar result is that when an IDD increases from 1.20 g cm^{-3} to 1.40 g cm^{-3}, the response time of VMC at the same location is delayed. However, this similarity does not apply to the position D. The reason is that the local soil sliding is found in the shallow layer in the position D of test 2. It can lead to the decrease in the part of the soil thickness. Thus, the position D of test 2 affected by the rainfall is earlier than that of test 1.

The stable value of VMC with an IDD of 1.20 g cm^{-3} is smaller than that of 1.40 g cm^{-3}. It is suitable for most of the depths of test 1 to test 4. The abnormal points include as follows: the depth of 0.5 m at C and D of test 1 and test 2, the depth of 0.1 m at A, B and C and the depth of 0.3 m at C of test 3 and test 4. This is due to the difference in soil – water action during rainfall. When rainfall intensity is 60 mm h^{-1}, all the rainwater can percolate through the soil with an IDD of 1.20 g cm^{-3} and 1.40 g cm^{-3}. However, when rainfall intensity is 90 mm h^{-1} and an IDD is 1.40 g cm^{-3}, the rainwater seepage capacity is less than 90 mm h^{-1}. Subsequently, rainwater cannot completely penetrate the soil and surface runoff is formed. The slope is eroded by surface runoff; it can be found in the macroscopic phenomena of test 4. Therefore, even if the rainfall intensity is 90 mm h^{-1}, the stable value of VMC is relative small. In addition, test 5 and test 6 have the same initial dry density, but the response time cannot decrease when the rainfall intensity is from 60 mm h^{-1} to 90 mm h^{-1}. The reasons are mentioned in the previous paragraph.
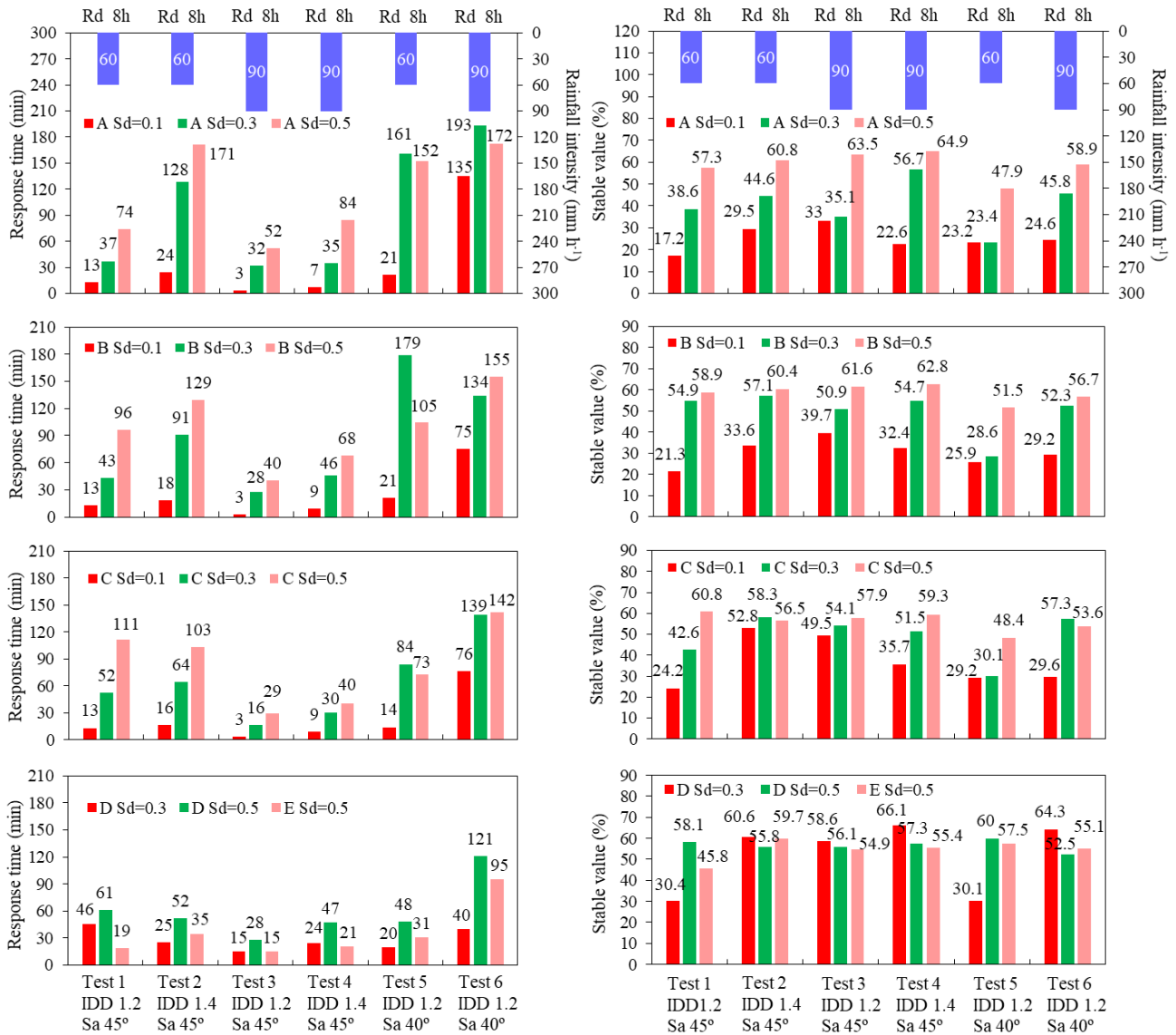
Figure 12. Response time and stable value of volume moisture content in six tests during the first rainfall.

3.3 Pore water pressure

Pore water pressure (PWP) at three positions (C, D, E) is shown in Figure 13-Figure 18. The sensor #3 of PWP in test 2 and test 4 breaks down, and it deviates from its original position in test 3. Thus, the PMP of the sensor #3 are not analyzed in this section. The variation of PWP mainly consists of similar three parts: stability, significant increase, dynamic fluctuation. Some differences between these tests can be clarified. In test 1, the PWP at a depth of 0.3 m at C fluctuates drastically during the first rain. However, the PWP of test 2 does not fluctuate, and its variation is smaller than that in test 1 (Fig. 13). In addition, the PWP with a depth of 0.3 m at D varies gently in test 1, but it increases significantly during the second and third rain in test 2. The fluctuation occurs at a depth of 0.5 m at D in test 1 (Fig. 14). The changes of PWP and VMC are not synchronized, which manifests in two aspects. One is the response time of PWP is later than that of VMC; the other is that VMC is in a stable stage when PWP fluctuates.
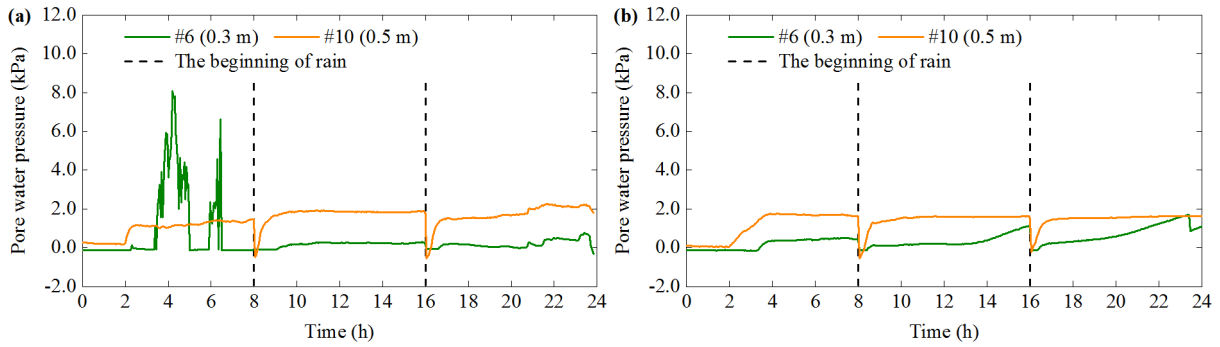
Figure 13. Pore water pressure in position C of (a) test 1 and (b) test 2.
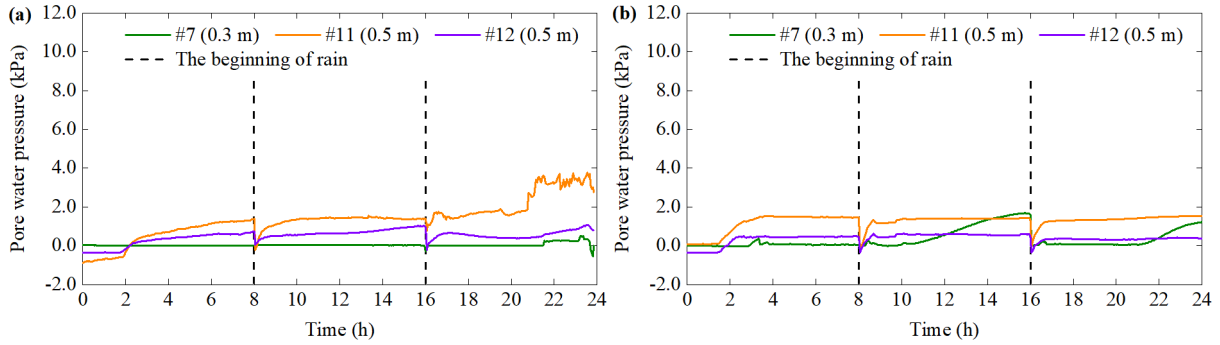
Figure 14. Pore water pressure in positions D and E of (a) test 1 and (b) test 2.

In the first rainfall, the PWP response time of test 3 is shorter than that of test 4 at the same location (Figs. 15 and 16). The difference in PWP response time is consistent with that in VMC. It directly reflects the soil seepage capacity when an IDD is 1.20 g cm^{-3} and 1.40 g cm^{-3} respectively. Besides, the frequent fluctuation of PWP mostly appears in test 3. In particular, PWP in test 3 is decreasing after increasing at the most locations except for the depth of 0.5 m of D. This downward trend exists at position C of test 4, but is not significant at D and E.
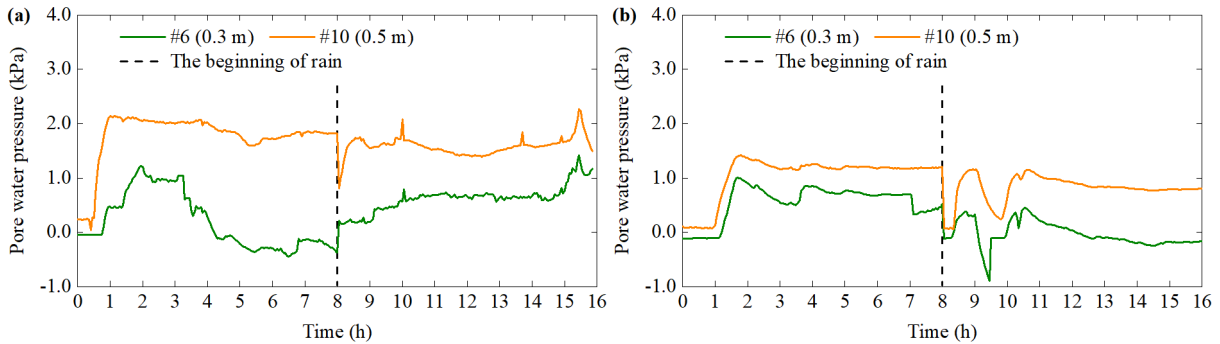
Figure 15. Pore water pressure in position C of (a) test 3 and (b) test 4.
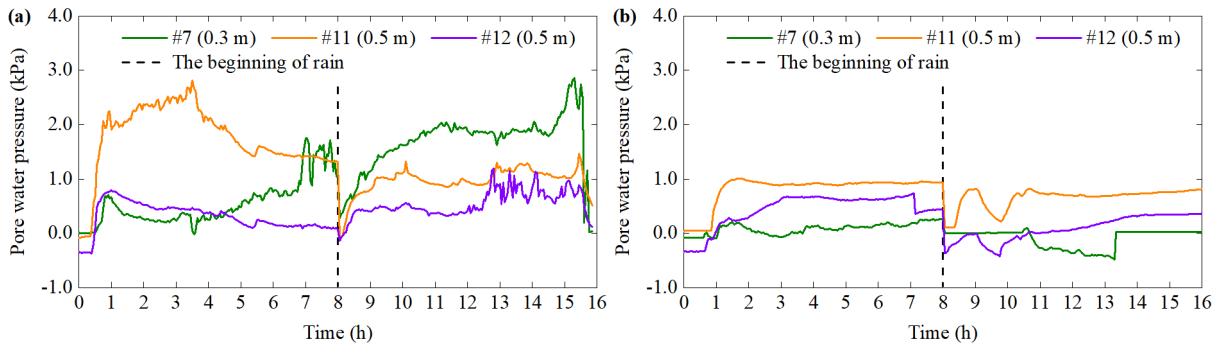
Figure 16. Pore water pressure in positions D and E of (a) test 3 and (b) test 4.

347   Figure 17-Figure 18 shows the differences between test 5 and test 6 during the first rainfall. One is
348   that the PWP curve at C in test 5 is flat. However, all the PWP in test 6 experiences the flat, increase
349   and decrease stages. The other is that PWP at E in test 5 has an obvious volatility characteristic. It
350   fluctuates to the peak at the end of the first rain. Whereas, PWP at E in test 6 has a downward trend
351   after it reaches the peak. This opposite trend is related to the differences between the soil failures of
352   these two tests. Soil sliding can cause stress to relax, which further results in an increase in soil
353   porosity. It will induce pore water pressure to decrease. When rainwater is enough, pore water
354   pressure can be restored.
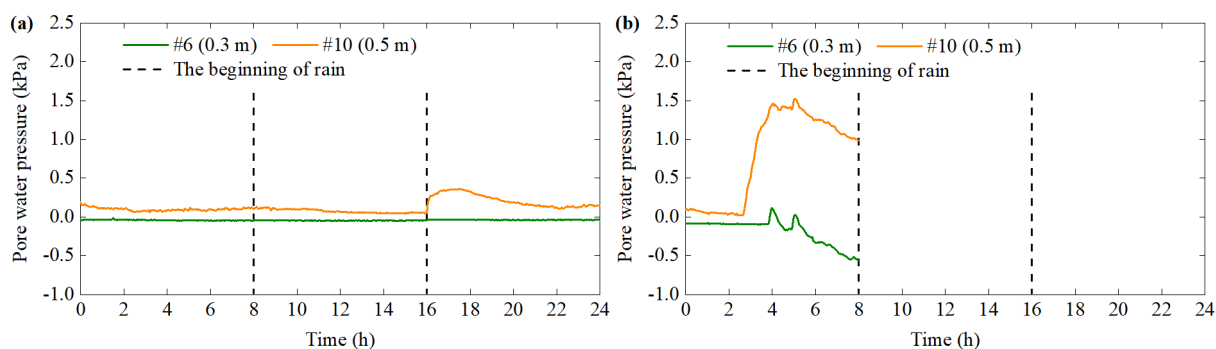
355
356   Figure 17. Pore water pressure in position C of (a) test 5 and (b) test 6.
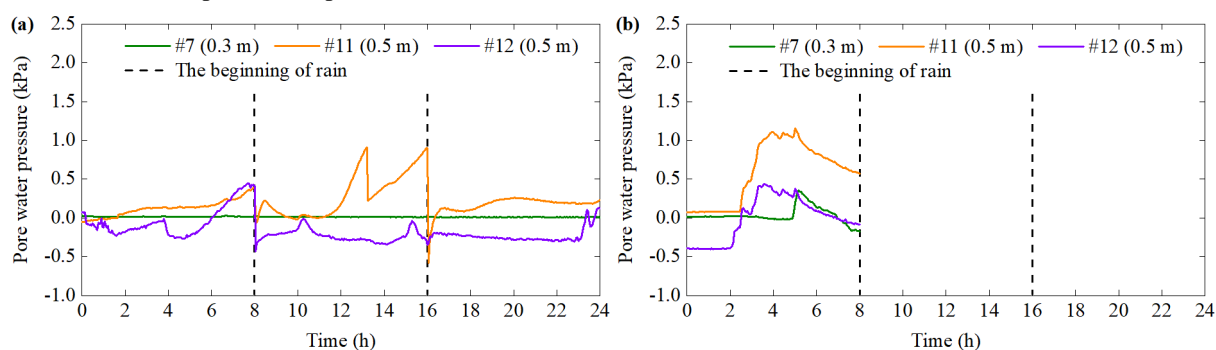
357
358   Figure 18. Pore water pressure in positions D and E of (a) test 5 and (b) test 6.

359   Figure 19 shows the response time and variation of PWP at five positions during the first rainfall.
360   Test 1and Test 2, Test 3 and Test 4 in Figure 19 are respectively compared. The main commonality is
361   that when the location and rainfall duration is same, the response time of PWP with an IDD of 1.20 g
362   cm^{-3} is shorter than that of 1.40 g cm^{-3}. Nonetheless, most of the variation in PWP has a contrary
363   pattern. The reason is that even if the rainfall intensity is the same, the slope with different density
364   has diverse hydrological characteristics (Lan et al., 2003). For example, the permeability of a slope
365   with a large density is relatively small, thus, the variation in PWP is restricted. A significant
366   difference is that although PWP change of the surface soil layer at each position is the smallest
367   except for test 3, the PWP changes of other two depths do not increase with the increase of depth.
368   The reasons are analyzed as follows. When the rainwater accumulates at a depth of 0.3 m, the PWP
369   variation is relative large. At this moment, the PWP with a depth of 0.3 m can be larger than that of
370   0.5 m. The continuous seepage can cause soil gravity to increase. It can produce the compressive
371   stress on the soil layer at a depth of 0.5 m. The further decrease in soil porosity can cause PWP to
372   increase. At the same time, if the soil with a depth of 0.3 m begins to slide, PWP will be released.
373   Therefore, in these conditions, the PWP with a depth of 0.5 m may be larger than that of 0.3 m. It
374   suggests that changes in PWP depend on soil deformation and its diffusion. This validates the study

375   by Iverson et al. (1997).
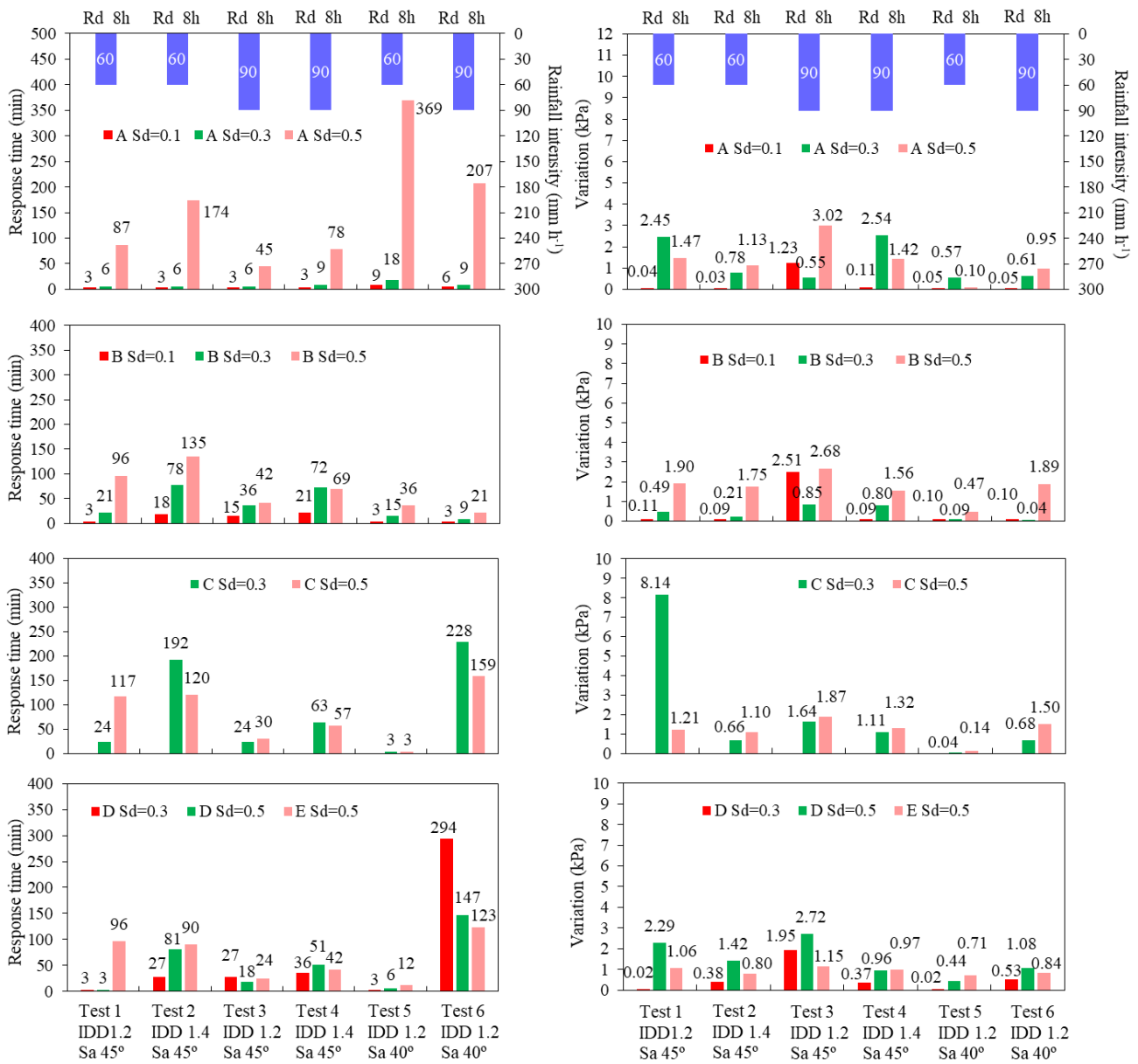
376
377   Figure 19. Response time and variation of pore water pressure in six tests during the first rainfall.

378   **4   Discussion**

379   Six model tests have commonness in the patterns of slope failure based on the macroscopic
380   phenomena. Based on these tests, the landslide formation can be classified into five stages and shown
381   in Table 2. They are basically consistent with the results of the field survey in Southeast Guangxi
382   (Wei et al., 2017). Therefore, the initiation processes of granite residual soil landslides can be
383   reproduced by flume model tests.

384   (i) Rain infiltration and crack generation. At the beginning of rainfall, all rainwater can seep into
385   the slope. There is no surface runoff on the slope. Volume moisture content begins to increase.
386   However, matrix suction decreases, which results in the reduction of shear strength. In addition, the
387   gravity load of the slope increases and favors the downward creep. The differential distribution of
388   soil strength can cause cracks to generate at the slope toe, which provide a preferential path for
389   rainwater.
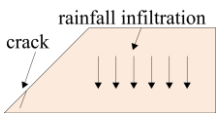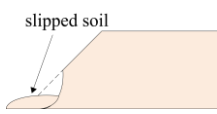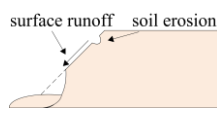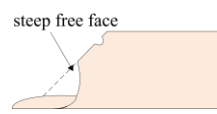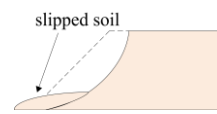
(ii) Soil slide at the slope toe. As rainfall continues, rainwater penetrates the soil through the crack. The accumulated rainwater in the crack can produce the pressure acting on the slope. It facilitates the propagation of the crack. Hence, the soil strength around the crack decreases. Meanwhile, the underground runoff converges at the toe of the slope. The VMC at the slope toe is relative large. The water pressure's difference between the top and toe of the slope increases. This difference in pressure and changes in the soil microstructure can lead to a reduction in the shear strength of the slope. Therefore, the soil at the foot of the slope softens and slides first. Subsequently, muddy water gradually flows out from the slope toe. This indicates that fine particles migrate through subsurface runoff, causing changes in the microstructure of some soils along the flow network.

(iii) Occurrence of surface runoff and soil erosion. The water content of shallow soil layer increases to a saturation value with the continuing rain. A saturation zone appears. This process allows fine particles to migrate vertically to a certain depth. Subsequently, the infiltration path will be blocked, and rainwater cannot permeate the soil smoothly. The surface runoff gradually forms. On the other hand, the gravel of the soil remains on the slope surface, which is conductive to seepage along the slope. Therefore, subsurface runoff can lead to the loss of the surface layer soil. Multiple low-lying areas and ditches are generated by the erosion of surface runoff and splash erosion of rainfall. The erosion destruction is most serious in the slope toe and the slope middle.

(iv) Formation of steep-free surface. As the soil at the foot of the slope continues to slide, the geometry and stress of the slope have changed due to the removal of downward support. Even the internal force balance of the slope is destroyed. The unstable range expands to the surroundings. A steep free surface begins to form subsequently. However, the soil on the top of the slope has not slipped.

(v) Soil slide at the upper slope. The presence of macro-pores between the gravel can promote the rainwater penetration through the soil. This process facilitates the rainwater transmission to a deep layer. The sliding force of the slope can be further improved. Meanwhile, the unbalance internal forces gradually increase due to the repeat slide of the slope toe. Besides, the increase of PWP leads to a reduction in the effective stress and shearing strength. Finally, when the sliding force is greater than the soil resistance, the soil at the slope top begins to slide. Obvious shear deformation is formed.

Table 2. Schematic diagrams and photos of the landslide formation

One difference between six tests is the time of landslide initiation (Table 3). Six initiation times are 50 min, 67 min, 32 min, 45 min, 26min and 5 min respectively. When the slope angle and rainfall

422 intensity are the same, the initiation time of a landslide with a density of 1.20 g cm^{-3} is shorter than
423 that of a landslide with a density of 1.40 g cm^{-3}. The difference is 17 min and 13 min. The reason is
424 that when the IDD increases, the slope permeability decreases (Lan et al., 2003), and the infiltration
425 process is relative slow. Therefore, the slope needs more penetration time. This corresponds to the
426 difference of the response time of VMC in section 3.2. In section 3.2, when an IDD increases from
427 1.20 g cm^{-3} to 1.40 g cm^{-3}, the response time of VMC and PWP is delayed. The decrease rate of the
428 shearing strength is correspondingly slow. This is beneficial to the stability of the slope. When the
429 slope angle and density are the same, the initiation time of a landslide with the rainfall intensity of 90
430 mm h^{-1} is 18 min-22 min shorter than that of a landslide with the rainfall intensity of 60 mm h^{-1}. The
431 reason is that when the rainfall intensity is relative larger, more rainwater can penetrate the soil
432 quickly. This leads to a rapid increase in VMC and PWP in shallow soil layers. The shearing strength
433 decreases. At this time, the difference of water pressure between the slope toe and the slope crest is
434 obvious, which result in the first soil sliding at the slope toe. Meanwhile, when the IDD is 1.20 g cm^{-3}
435 , the rainfall intensity is 60 mm h^{-1} and 90 mm h^{-1}, if a slope angle increases from 40º to 45º, the
436 starting time can be delayed by 24 min and 27 min. This is because steep slopes are not conducive to
437 infiltration of rainwater (Xu et al., 2018). Hence, the VMC and PWP respond to rainfall slowly,
438 which is favorable to slope stability. In a word, the initiation time of landslide is closely related to
439 density, slope angle, and rainfall intensity. It is mainly controlled by the hydrological response of the
440 slope.

441 Table 3. Initiation time of landslide for six tests.

Test number	1	2	3	4	5	6
Initiation time (min)	50	67	32	45	26	5

442

443 The other difference in six tests is the failure mode and process of landslide. In test 1, all the
444 surface soil slips, and the frequent sliding soil is in the shape of a block. In test 2, the sliding area
445 slowly spreads to the surroundings, and the partial right shoulder fails to slide eventually. In test 3,
446 the soil around the crack slides quickly, and all the soil on the slope surface is destroyed. In test 4, the
447 scouring action of rain results in the formation of a deep gully, but the slope has stabilized finally. In
448 test 5, the low-lying areas are enlarged with the continuous rainfall, and all the soil at the slope toe
449 slips suddenly. In test 6, the soil surrounding crack slide rapidly, and the soil failure are repetitive.
450 The above mentioned macroscopic phenomenon contains two main characteristics. When the IDD is
451 1.20 g cm^{-3}, tensile crack is an important triggering factor for soil failure, and the formation process
452 of landslide is relatively sudden and large in scale. When the IDD is 1.40 g cm^{-3}, soil failure of the
453 slope foot can trigger the trailing edge slip. Therefore, the sliding process is gradual and small-scale,
454 often accompanied by the appearance of low-lying areas and ditches. The main reason is required
455 energy for the destruction of large density is significantly greater than that of small density (Xu et al.,
456 2018). Hence, the formation process of landslide is different due to the initial state of the slope.
457 Section 3.3 shows that the pore water pressure fluctuates significantly during the soil failure.
458 However, the variation of pore water pressure at the same position and depth is not synchronized
459 with the water content. The typical periods of test 2 and the test 3 are selected in this section to
460 understand the relationship between them. In test 2 with an IDD of 1.40 g cm^{-3}, when the rainfall
461 lasts for 195-225 minutes, the soil in the slope middle slides. It promotes the development of cracks

462 and causes massive soil on the slope to slide (Fig. 20a). The seventh sensor is the closest to unstable
463 soil, thus, the data of this sensor is selected for detailed analysis. Figure 20b shows that the water
464 content is stable at about 61.6 % during this period, and the soil is in an over-saturated state; however,
465 pore water pressure gradually increases to a peak of 0.361 kPa when the rainfall duration is 195-201
466 minutes. Subsequently, pore water pressure decreases rapidly, and maintains a certain degree of
467 volatility. When the rainfall duration is 210 minutes, pore water pressure begins to increase again. In
468 test 3 with an IDD of 1.20 g cm^{-3}, when the rainfall lasts for 30-48 minutes, the shallow soil is
469 softened and slides many times (Fig. 21a). Figure 21b shows that when the rainfall duration is 30-36
470 minutes, VMC and PWP both increases; when the rainfall lasts for 36 minutes, the increasing trend
471 of them is relatively gentle; when the rainfall lasts for 42 minutes, although PWP increases rapidly
472 again, but VMC remains stable at 58.7 %. In a word, the differences in the variation of PWP and
473 VMC comprise two aspects. One is that when VMC begins to increase, PWP is invariant. The
474 response time of PWP is behind that of VMC. The other is that when VMC is constant or is in a
475 significant rise, PWP has almost no change or only dramatic fluctuations. These may be related to
476 mechanical behavior of granite residual soil.
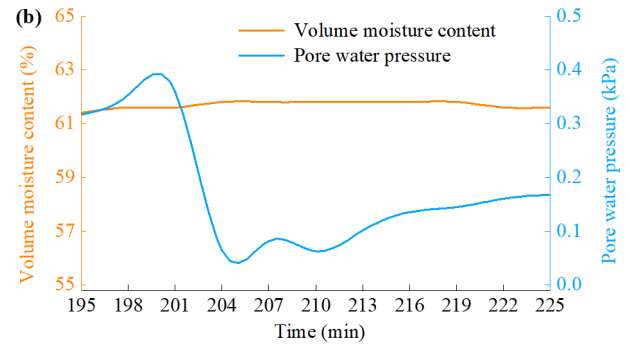
477

478 Figure 20. Typical phenomenon and result with an initial dry density of 1.40 g cm^{-3}. (a) Slope failure. (b) Results for
479 sensor #7 closest to sliding surface.
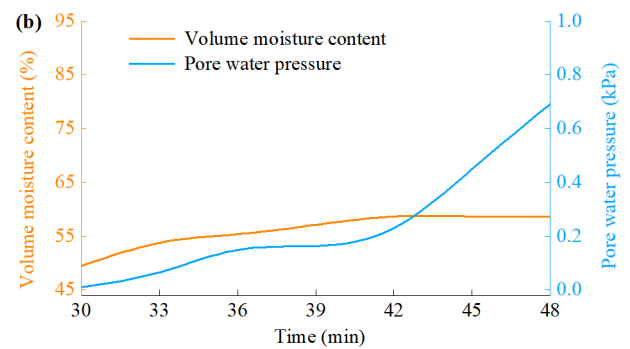
480

481 Figure 21. Typical phenomenon and result with an initial dry density of 1.20 g cm^{-3}. (a) Slope failure. (b) Results of
482 sensor #7 closest to sliding surface .

483

484 The above results may be explained by the research made by Iverson (Iverson, 2005; Iverson et al.,
485 2000). He found that landslide mobilization is affected by mechanical properties of the shear zone
486 related to the initial density. When dry density is low and rainfall intensity is high, the "hammering"
487 effect of rain can squeeze the shallow soil. In addition, pore water pressure can increase due to the
488 decrease in void ratio and leads to a reduction in shear strength. When the initial local shear
489 deformation occurs, the shear zone is mainly contractive. At the same time, excessive pore water

490   pressure is generated. However, excess pore water pressure is difficult to dissipate completely in a
491   short time, which can promote the continuous increase of pore water pressure and the connection of
492   potential sliding surfaces. Therefore, the type of landslide failure is a sudden sliding type in the
493   macroscopic phenomenon (Dai et al., 1999a; Dai et al., 1999b; Mckenna et al., 2011). When the dry
494   density is larger, the infiltration rate of rainwater is smaller. At the same time, the response time of
495   water content and pore water pressure is delayed, and the fluctuation of pore water pressure is limited.
496   As a result, the ability of the slope to resist seepage damage is improved effectively. When dilative
497   shear deformation appears, it can cause pore water pressure to dissipate, and even leads to the
498   occurrence of negative pore water pressure (Chen et al., 2018). It can results in the delay of the VMC
499   and the recovery of the shear strength. After that, long-term rainfall can restore the loss of pore
500   pressure due to soil dilation, and shear deformation will reappear. At this time, the macroscopic
501   phenomenon of landslide start is progressive (Dai et al., 1999a; Dai et al., 1999b; Mckenna et al.,
502   2011). The landslide mobilization mode in this paper is consistent with the above mentioned.

503   **5   Conclusion**

504   The present study is executed to analyze the failure mode and process of granite residual soil
505   landslides in Guangxi province, China. The following conclusions can be summarized.

506   (1) Volume moisture content and pore water pressure exhibits a non-synchronous response to the
507   rain. Initial dry density and rainfall intensity has a significant effect on the hydrological response.
508   Large density can restrain the rainwater infiltration rate and limit the fluctuation of pore water
509   pressure. In addition, high rainfall intensity is corresponding to the short response time of volume
510   moisture content. However, this is unsuitable for the soil with a small density, because the change of
511   soil microstructure alters the seepage path. The fluctuation of pore water pressure depends on soil
512   mechanical behavior and its diffusion.

513   (2) The differences in the formation process of granite residual soil landslides include the initiation
514   time and mode. The starting time of landslide is closely related to initial dry density, slope angle, and
515   rainfall intensity. It is mainly controlled by the hydrological response of the slope. The initiation time
516   of 1.20 g cm^{-3} is 13-17 min earlier than that of 1.40 g cm^{-3}. The initiation time of 90 mm h^{-1} is 18
517   min-22 min shorter than that of 60 mm h^{-1}. Mechanical properties of the shear zone play the
518   important role in the failure modes of landslides, which are closely related to the initial dry density.
519   Two failure modes can be observed. One is a sudden sliding in a large scale with a density of 1.2 g
520   cm^{-3}; the other is a progressive sliding in a small scale with a density of 1.40 g cm^{-3}.

521   (3) Landslide mobilization can be classified into five stages as follows: rain infiltration and crack
522   generation, soil slide at the slope toe, occurrence of surface runoff and soil erosion, formation of
523   steep-free surface, and soil slide at the upper slope. It is accompanied by the migration of fine
524   particles, and the formation of crack and macro-pores. Cracks and macro-pores can facilitate the
525   hydrological response in the deep layer.

526   Future research includes four aspects. Firstly, more tests involving multiple factors will be
527   conducted through the orthogonal experimental design. Secondly, triaxial instrument will be used to
528   perform the stress path tests. Thirdly, the influence of variation along the vertical direction of initial
529   dry density on slope failure will be analyzed. Fourthly, the quantitative relationship between volume
530   moisture content and pore water pressure during landslide initiation will be explored.

531

532 **Competing interests**

533 The authors declare that they have no conflict of interest.

534 **Acknowledgements**

535 This research was funded by the National Natural Science Foundation of China (No. 41901132,
536 51609041), the Natural Scientific Project of Guangxi Zhuang Autonomous Region (No.
537 2021GXNSFBA220025).
538

539 **References**

540 Calcaterra, D. and Parise, M.: Landslide types and their relationships with weathering in a Calabrian
541 basin, southern Italy, B. Eng. Geol. Environ., 64, 193-207, https://doi.org/10.1007/s10064-004-
542 0262-5, 2005.

543 Chang, Z., Huang, F., Huang, J., Jiang, S., Zhou, C., and Zhu, L.: Experimental study of the failure
544 mode and mechanism of loess fill slopes induced by rainfall, Eng. Geol., 280, 1-16,
545 https://doi.rog/10.1016/j.enggeo.2020.105941, 2021.

546 Chen, D. and Gong, X.: Experiment and modeling of soil-water characteristic curve of unsaturated
547 residual soil, Rock and Soil Mechanics, 35, 1885-1891, 2014 (in Chinese).

548 Chen, G., Meng, X., Qiao, L., Zhang, Y., and Wang, S.: Response of a loess landslide to rainfall:
549 observations from a field artificial rainfall experiment in Bailong River Basin, China, Landslides,
550 15, 895-911, https://doi.org/10.1007/s10346-017-0924-6, 2018.

551 Chen, H., Lee, C. F., and Law, K. T.: Causative mechanisms of rainfall-induced fill slope failures, J.
552 Geotech. Geoenviron. Eng., 130, 593-602, https://doi.org/10.1061//asce/1090-
553 0241/2004/130:6/593, 2004.

554 Chen, N., Zhu, Y., Huang, Q., Iqbal, J., Deng, M., and He, N.: Mechanisms involved in triggering
555 debris flows within a cohesive gravel soil mass on a slope: a case in SW China, J. Mt. Sci., 14,
556 611-620, https://doi.org/10.1007/s11629-016-3882-x, 2017.

557 Chen, X., Zhou, Q., and Cai, X.: Physical properties and shear strength characteristics of high liquid
558 limit granite residual soil, Chinese Journal of Geotechnical Engineering, 32, 901-908, 2011 (in
559 Chinese).

560 Coutinho, R. Q., Silva, M. M., dos Santos, A. N., and Lacerda, W. A.: Geotechnical characterization
561 and failure mechanism of landslide in granite residual soil, J. Geotech. Geoenviron. Eng., 145, 1-
562 16, https://doi.org/10.1061/(asce)gt.1943-5606.0002052, 2019.

563 Dahal, R. K., Hasegawa, S., Nonomura, A., Yamanaka, M., Masuda, T., and Nishino, K.: Failure
564 characteristics of rainfall-induced shallow landslides in granitic terrains of Shikoku Island of Japan,
565 Environ. Geol., 56, 1295-1310, https://doi.org/10.1007/s00254-008-1228-x, 2008.

566 Dai, F., Lee, C. F., and Wang, S.: Analysis of rainstorm-induced slide-debris flows on natural terrain
567 of Lantau Island, Hong Kong, Eng. Geol., 51, 279-290, https://doi.org/10.1016/s0013-
568 7952(98)00047-7, 1999a.

569 Dai, F., Lee, C. F., Wang, S., and Feng, Y.: Stress-strain behaviour of a loosely compacted voleanic-
570 derived soil and its significance to rainfall-induced fill slope failures, Eng. Geol., 53, 359-370,
571 https://doi.org/10.1016/s0013-7952(99)00016-2, 1999b.

572 Elkamhawy, E., Wang, H., Zhou, B., and Yang, Z.: Failure mechanism of a slope with a thin soft

band triggered by intensive rainfall, Environ. Earth. Sci., 77, 340-354, https://doi.org/10.1007/s12665-018-7538-8, 2018.

Fang, H., Cui, P., Pei, L., and Zhou, X.: Model testing on rainfall-induced landslide of loose soil in Wenchuan earthquake region, Nat. Hazard. Earth. Sys., 12, 527-533, https://doi.org/10.5194/nhess-12-527-2012, 2012.

Fu, R., Hu, X., Zhou, B., Wang, H., and Wang, J.: A quantitative characterization method of 3D morphology of sand particles, Rock and Soil Mechanics, 39, 483-490, 2018 (in Chinese).

Gasmo, J. M., Rahardjo, H., and Leong, E. C.: Infiltration effects on stability of a residual soil slope, Comput. Geotech., 26, 145-165, https://doi.org/10.1016/s0266-352x(99)00035-x, 2000.

Hu, H., Wang, A., Liu, Y., and Zhao, X.: Stability of granite soil high slopes, Chinese Journal of Geotechnical Engineering, 31, 824-828, 2009 (in Chinese).

Huang, C.-C. and Yuin, S.-C.: Experimental investigation of rainfall criteria for shallow slope failures, Geomorphology, 120, 326-338, https://doi.org/10.1016/j.geomorph.2010.04.006, 2010.

Huang, C.-C., Lo, C.-L., Jang, J.-S., and Hwu, L.-K.: Internal soil moisture response to rainfall-induced slope failures and debris discharge, Eng. Geol., 101, 134-145, https://doi.org/10.1016/j.enggeo.2008.04.009, 2008.

Igwe, O. and Fukuoka, H.: The effect of water-saturation on the stability of problematic slopes at the Iva Valley area, Southeast Nigeria, Arab. J. Geosci., 8, 3223-3233, https://doi.org/10.1007/s12517-014-1398-7, 2014.

Iverson, R. M.: Regulation of landslide motion by dilatancy and pore pressure feedback, J. Geophys. Res-Earth., 110, 1-16, https://doi.org/10.1029/2004JF000268, 2005.

Iverson, R. M., Reid, M. E., and LaHusen, R. G.: Debris-flow mobilization from landslides, Annu. Rev. Earth Pl. Sc., 25, 85-138, https://doi.org/10.1146/annurev.earth.25.1.85, 1997.

Iverson, R. M., Reid, M. E., Iverson, N. R., LaHusen, R. G., and Logan, M.: Acute sensitivity of landslide rates to initial soil porosity, Science, 290, 513-516, https://doi.org/10.1126/science.290.5491.513, 2000.

Jiang, Y., Chen, W., Wang, G., Sun, G., and Zhang, F.: Influence of initial dry density and water content on the soil-water characteristic curve and suction stress of a reconstituted loess soil, B. Eng. Geol. Environ., 76, 1085-1095, https://doi.org/10.1007/s10064-016-0899-x, 2017.

Jiao, J., Wang, X., and Nandy, S.: Confined groundwater zone and slope instability in weathered igneous rocks in Hong Kong, Eng. Geol., 80, 71-92, https://doi.org/10.1016/j.enggeo.2005.04.002, 2005.

Kassim, A., Gofar, N., Lee, L. M., and Rahardjo, H.: Modeling of suction distributions in an unsaturated heterogeneous residual soil slope, Eng. Geol., 131-132, 70-82, https://doi.org/10.1016/j.enggeo.2012.02.005, 2012.

Kim, J., Jeong, S., Park, S., and Sharma, J.: Influence of rainfall-induced wetting on the stability of slopes in weathered soils, Eng. Geol., 75, 251-262, https://doi.org/10.1016/j.enggeo.2004.06.017, 2004.

Kim, M. S., Onda, Y., Kim, J. K., and Kim, S. W.: Effect of topography and soil parameterisation representing soil thicknesses on shallow landslide modelling, Quatern. Int., 384, 91-106, https://doi.org/10.1016/j.quaint.2015.03.057, 2015.

Lacerda, W. A.: Landslide initiation in saprolite and colluvium in southern Brazil: Field and

laboratory observations, Geomorphology, 87, 104-119, https://doi.org/10.1016/j.geomorph.2006.03.037, 2007.

Lan, H., Zhou, C., Lee, C. F., Wang, S., and Wu, F.: Stability response analysis of rainfall landslide under instantaneous pore water pressure: a case study of natural rainfall landslide in Hong Kong, Science in China Ser. E Technological Sciences, 119-136, 2003 (in Chinese).

Lee, I.-M., Sung, S.-G., and Cho, G.-C.: Effect of stress state on the unsaturated shear strength of a weathered granite, Can. Geotech. J., 42, 624-631, https://doi.org/10.1139/t04-091, 2005.

Li, Z., Tang, L., and Sang, H.: 3-D micro-structure of the particle and water morphology of the granite residual soil, Acta Scientiarum Naturalium Universitatis Sunyatseni, 56, 15-21, 2017 (in Chinese).

Liang, H., He, S., Lei, X., Bi, Y., Liu, W., and Ouyang, C.: Dynamic process simulation of construction solid waste (CSW) landfill landslide based on SPH considering dilatancy effects, B. Eng. Geol. Environ., 2, 1-15, https://doi.org/10.1007/s10064-017-1129-x, 2017.

Liao, L., Yang, Y., Yang, Z., Zhu, Y., Hu, J., and Zou, D. H. S.: Mechanical state of gravel soil in mobilization of rainfall-induced landslides in the Wenchuan seismic area, Sichuan province, China, Earth Surf. Dynam., 6, 637-649, https://doi.org/10.5194/esurf-6-637-2018, 2018.

Liao, L., Zhu, Y., Zhao, Y., Wen, H., Yang, Y., Chen, L., Ma, S., and Xu, Y.: Landslide integrated characteristics and susceptibility assessment in Rongxian county of Guangxi, China, J. Mt. Sci., 16, 657-676, https://doi.org/10.1007/s11629-017-4804-2, 2019.

Lin, H., Yu, Y., Li, G., and Peng, J.: On application of soil-water characteristic curves to landslide forecast, Chinese Journal of Rock Mechanics and Engineering, 2569-2576, 2009 (in Chinese).

Liu, W., Song, X., Luo, J., and Hu, L.: The processes and mechanisms of collapsing erosion for granite residual soil in southern China, J. Soil. Sediment., 20, 992-1002, https://doi.org/10.1007/s11368-019-02467-4, 2020a.

Liu, W., Ouyang, G., Luo, X., Luo, J., Hu, L., and Fu, M.: Moisture content, pore-water pressure and wetting front in granite residual soil during collapsing erosion with varying slope angle, Geomorphology, 362, 1-10, https://doi.org/10.1016/j.geomorph.2020.107210, 2020b.

Liu, X., Zhang, X., Kong, L., Li, X., and Wang, G.: Effect of cementation on the small-strain stiffness of granite residual soil, Soils. Found., 61, 520-532, https://doi.org/10.1016/j.sandf.2021.02.001, 2021.

Lu, Y., Wei, C., Cai, G., and Zhao, C.: Water-holding characteristics of weathered granite soils, Chinese Journal of Geotechnical Engineering, 40, 96-100, 2018 (in Chinese).

Luo, X., Gao, H., He, P., and Liu, W.: Experimental investigation of dry density, initial moisture content, and temperature for granite residual soil disintegration, Arab. J. Geosci., 14, 1-9, https://doi.org/10.1007/s12517-021-07239-4, 2021.

McKenna, J. P., Santi, P. M., Amblard, X., and Negri, J.: Effects of soil-engineering properties on the failure mode of shallow landslides, Landslides, 9, 215-228, https://doi.org/10.1007/s10346-011-0295-3, 2011.

Ministry of Construction of the People's Republic of China: Code for investigation of geotechnical engineering (GB50021-2001), China Architecture & Building Press, Beijing, 2002 (in Chinese).

Moriwaki, H., Inokuchi, T., Hattanji, T., Sassa, K., Ochiai, H., and Wang, G.: Failure processes in a full-scale landslide experiment using a rainfall simulator, Landslides, 277-287,

657   https://doi.org/10.1007/s10346-004-0034-0, 2004.

658 Mukhlisin, M. and Taha, M. R.: Numerical model of antecedent rainfall effect on slope stability at a
659   hillslope of weathered granitic soil formation, J. Geol. Soc. India., 79, 525-531,
660   https://doi.org/10.1007/s12594-012-0077-0, 2012.

661 Mukhlisin, M., Taha, M. R., and Kosugi, K.: Numerical analysis of effective soil porosity and soil
662   thickness effects on slope stability at a hillslope of weathered granitic soil formation, Geosci. J., 12,
663   401-410, https://doi.org/10.1007/s12303-008-0039-0, 2008.

664 Ng, C. W. and Pang, Y. W.: Experimental investigations of the soil-water characteristics of a
665   volcanic soil, Can. Geotech. J., 37, 1252-1264, https://doi.org/10.1139/t00-056, 2000.

666 Pham, K., Kim, D., Lee, I.-M., and Choi, H.: Hydraulic-mechanical properties of unsaturated granite-
667   weathered residual soil in Korea, Vadose. Zone. J, 18, 1-13,
668   https://doi.org/10.2136/vzj2018.10.0188, 2019.

669 Qu, Y., Ng, C. W., and Shang, Y.: Study on latitudinal effect on lateritization of eluvial soil on
670   granite and cuase for weak lateritization of the soil in Hong Kong, Journal of Engineering Geology,
671   16-20, 2000 (in Chinese).

672 Rahardjo, H., Leong, E. C., and Rezaur, R. B.: Effect of antecedent rainfall on pore-water pressure
673   distribution characteristics in residual soil slopes under tropical rainfall, Hydrol. Process., 22, 506-
674   523, https://doi.org/10.1002/hyp.6880, 2008.

675 Rahardjo, H., Aung, K. K., Leong, E. C., and Rezaur, R. B.: Effects of pore-size distribution on
676   engineering properties of residual soils, in: Proceedings of the Second World Engineering
677   Congress, Geotechnical Engineering & Transportation, Sarawak, Malaysia, 22-25 July 2002, 70-
678   76, 2002.

679 Rahardjo, H., Lee, T. T., Leong, E. C., and Rezaur, R. B.: Response of a residual soil slope to rainfall,
680   Can. Geotech. J., 42, 340-351, https://doi.org/10.1139/t04-101, 2005.

681 Rahardjo, H., Satyanaga, A., Leong, E.-C., Ng, Y. S., and Pang, H. T. C.: Variability of residual soil
682   properties, Eng. Geol., 141-142, 124-140, https://doi.org/10.1016/j.enggeo.2012.05.009, 2012.

683 Rahman, A. S. A., Noor, M. J. M., Jais, I. B. M., Sidek, N., and Ahmad, J.: Shear strength of granitic
684   residual soil in saturated and unsaturated conditions, in: AIP Conference Proceedings, Advances in
685   Civil Engineering and Science Technology, Penang, Malaysia, 5-6 September 2018, 1-9, 2018.

686 Rezaur, R. B., Rahardjo, H., Leong, E. C., and Lee, T. T.: Hydrologic behavior of residual soil slopes
687   in Singapore, J. Hydrol. Eng., 8, 133-144, https://doi.org/10.1061/(asce)1084-0699(2003)8:3(133),
688   2003.

689 Shu, R., Kong, L., Liu, B., and Wang, J.: Stress-strain strength characteristics of undisturbed granite
690   residual soil considering different patterns of variation of mean effective stress, Appl. Sci-Basel.,
691   11, 1-16, https://doi.org/10.3390/app11041874, 2021.

692 Take, W. A., Bolton, M. D., Wong, P. C. P., and Yeung, F. J.: Evaluation of landslide triggering
693   mechanisms in model fill slopes, Landslides, 1, 173-184, https://doi.org/10.1007/s10346-004-
694   0025-1, 2004.

695 Tu, X. B., Kwong, A. K. L., Dai, F. C., Tham, L. G., and Min, H.: Field monitoring of rainfall
696   infiltration in a loess slope and analysis of failure mechanism of rainfall-induced landslides, Eng.
697   Geol., 105, 134-150, https://doi.org/10.1016/j.enggeo.2008.11.011, 2009.

698 Wang, G. and Sassa, K.: Factors affecting rainfall-induced flowslides in laboratory flume tests,

699   Geotechnique, 51, 587-599, https://doi.org/10.1680/geot.51.7.587.51386, 2001.

700 Wang, Z., Mai, T., and Qi, C.: Shear strength and microstructure of compacted granite residual soils
701   in Rong County, Hydrogeology & Engineering Geology, 45, 101-107, 2018 (in Chinese).

702 Wei, C., Wen, H., Liao, L., Yang, Y., Ma, S., Zhao, Y., and Chen, L.: Failure characteristics and
703   prevention measures of granite residual soil slope in the southeast of Guangxi Province, China,
704   Earth and Environment, 45, 576-586, 2017 (in Chinese).

705 Wen, H.: A detailed survey report of geological disasters in Rongxian County, Guangxi., Guangxi
706   Zhuang Autonomous Region Geological Environmental Monitoring Station, Guilin, Guangxi., 196
707   pp., 2015 (in Chinese).

708 Wu, N.: Engineering characteristics of cutting slope of granite residual soil, Mountain Research, 24,
709   431-436, 2006a (in Chinese).

710 Wu, N.: Study on classification of granite residual soils, Rock and Soil Mechanics, 27, 2299-2304,
711   2006b (in Chinese).

712 Xia, J., Cai, C., Wei, Y., and Wu, X.: Granite residual soil properties in collapsing gullies of south
713   China: spatial variations and effects on collapsing gully erosion, Catena, 174, 469-477,
714   https://doi.org/10.1016/j.catena.2018.11.015, 2019.

715 Xu, X. and Jian, W.: Experiment study on rainfall infiltration of slope under thrust at front end, Rock
716   and Soil Mechanics, 38, 3547-3554, 2017 (in Chinese).

717 Xu, X., Jian, W., and Wu, N.: Influence of repeated wetting cycles on shear properties of natural
718   residual soil China J. Highw. Transp., 30, 33-40, 2017 (in Chinese).

719 Xu, X., Jian, W., Wu, N., Xu, X., and Liu, J.: Unsaturated seepage characteristics of slope under
720   rainfall infiltration, Earth Science, 43, 922-932, 2018 (in Chinese).

721 Yao, Y., Ni, J., and Li, J.: Stress-dependent water retention of granite residual soil and its
722   implications for ground settlement, Comput. Geotech., 129, 1-11,
723   https://doi.org/10.1016/j.compgeo.2020.103835, 2021.

724 Zhai, Q., Rahardjo, H., and Satyanaga, A.: Variability in unsaturated hydraulic properties of residual
725   soil in Singapore, Eng. Geol., 209, 21-29, https://doi.org/10.1016/j.enggeo.2016.04.034, 2016.

726 Zhan, L., Jia, G., Chen, Y., and Fredlund, D. G.: Analytical solution for rainfall infiltration into
727   infinite long slopes considering properties of unsaturated soil, Chinese Journal of Geotechnical
728   Engineering, 1214-1220, 2010 (in Chinese).

729 Zhan, L., Li, H., Chen, Y., and Fredlund, D. G.: Parametric analyses of intensity-duration curve for
730   predicting rainfall-induced landslides in residual soil slope in Southeastern coastal areas of China,
731   Rock and Soil Mechanics, 33, 872-880+886, 2012 (in Chinese).

732 Zhang, S. and Tang, H.: Experiment study of disintegration mechanism for unsaturated granite
733   residual soil, Rock and Soil Mechanics, 34, 1668-1674, 2013 (in Chinese).

734 Zhang, W. G., Zhang, R. H., Han, L., and Goh, A. T. C.: Engineering properties of the Bukit Timah
735   Granitic residual soil in Singapore, Underground Space, 4, 98-108,
736   https://doi.org/10.1016/j.undsp.2018.07.001, 2019.

737 Zhao, X. and Hu, H.: Investigation on failure of granitic residual slope by using centrifugal model
738   test, Journal of Engineering Geology, 13, 410-414, 2005 (in Chinese).

739 Zhao, Y., Sun, X., Wen, T., Chen, R., and Huang, L.: Micro-structural evolution of granite residual
740   soil under external loading based on X-ray micro-computed tomography, Ksce. J. Civ. Eng., 25,

741  2836-2846, https://doi.org/10.1007/s12205-021-0803-5, 2021.

742 Zhou, J., Du, Q., Li, Y., and Zhang, J.: Centrifugal model tests on formation mechanism of landslide-

743  type debris flows of cohesiveless soils, Chinese Journal of Geotechnical Engineering, 36, 2010-

744  2017, 2014 (in Chinese).

745 Zhu, J.-H. and Anderson, S. A.: Determination of shear strength of Hawaiian residual soil subjected

746  to rainfall-induced landslides, Geotechnique, 48, 73-82, https://doi.org/10.1680/geot.1998.48.1.73,

747  1998.

748 Zuo, C., Xu, Y., Ding, S., and Tang, X.: Class soil landslide stability and its influencing factor

749  interaction law, Research of Soil and Water Conservation, 22, 325-330, 2015 (in Chinese).

750